AN ANALYSIS OF ERUPTION STYLES IN LUNAR FLOOR-FRACTURED CRATERS. L. M. Jozwiak[1], J. W. Head[1], and L. Wilson[2,1] [1]Dept. Earth, Environmental and Planetary Sciences, Brown University, Providence, RI 02912.[2]Lancaster Environment Centre, Lancaster University, Lancaster LA1 4YQ, UK
(lauren_jozwiak@brown.edu)

Introduction: Lunar floor-fractured craters are a set of 170 craters that have uplifted, fractured floors, and numerous associated morphologies including volcanic morphologies such as mare deposits and pyroclastic deposits [1, 2]. The craters are predominately located near the edges of large lunar basins and in association with lunar mare deposits [1, 2]. Morphologic analysis of these craters suggests that the deformation is the result of magmatic intrusion beneath the crater floor [2]. During this process, a dike propagates from depth, stalls in the brecciated shallow subsurface lens beneath the crater, forms a sill, and then the magma continues to evolve, occasionally producing subsequent explosive deposits [2, 3]. The temporal relationships of the magmatic evolution processes to the sill formation processes have thus far been unexplored, including how these processes affect the eruption style associated with the formation of the volcanic morphologies.

Lunar Pyroclastic Deposits: Pyroclastic deposits on the Moon are classically divided into two size categories: regional deposits with areas > 1000 km^2, and localized deposits with areas < 1000 km^2 [e.g. 4]. In addition to being areally extensive, the regional pyroclastic deposits typically lack observable vent structures, which may have been covered by younger deposits [5, 6]. Conversely, most localized deposits have an identifiable vent structure and are surrounded by a low-albedo annulus of inferred pyroclastic material [5]. These different morphologies have led to interpretations of different eruption styles for these two broad categories of deposit. Regional pyroclastic deposits have been inferred to form by continuous Hawaiian-style fire-fountaining eruptions [e.g. 7]. In contrast, the localized pyroclastic deposits have been assumed to form by more intermittent vulcanian-style eruptions [8].

A classic example of the localized pyroclastic deposit setting is in the crater Alphonsus (Fig. 1) (D = 119 km) (13.4° S, 2.8° W). This crater hosts 11 classically recognized pyroclastic vents and deposits with clearly visible low-albedo annuli [8]; additionally the crater hosts 2 recently identified smaller vents with intermediate albedo annuli [9]. The differences between these two deposit styles, in addition to compositional diversity amongst the deposits [10], suggest at least local variations in the magmatic evolution of the intrusion and the venting process.

Humboldt Crater: In an effort to explore further the relationship between intrusion formation and intrusion degassing and venting, we performed a detailed morphologic analysis of the archetypal floor-fractured crater Humboldt (Fig. 2) (D = 208 km) (27.2° S, 80.9° E) [11]. Utilizing Kaguya Terrain Camera [12] images and a Kaguya Terrain Camera (TC) DEM co-registered to the Lunar Orbiter Laser Altimeter (LOLA) geodetic framework [13], we analyzed the fracture morphologies within Humboldt crater. We identified four fracture morphologies: graben, "v" fracture, "shallow v" fracture, and pit chain. Additionally, we identified a previously unrecognized vent morphology located along several of the "shallow v" fractures. The previously identified volcanic morphologies within Humboldt crater are four large mare deposits (~1300 km^2, 500 km^2, 225 km^2, and 150 km^2); additionally, Gaddis et al. (2003) [5] identified possible signatures of pyroclastic deposits associated with each of the mare ponds. The pyroclastic deposits lack source vents, and are spread diffusely across the mare deposits making determinations about the total areal extent difficult [5]. The mare deposits are located along, and in some places embay segments of the graben-style fractures; although, the mare are never cut by fractures. We interpret these features to form from dikes that propagate from the bending edge of the sill [14]. Where the dike reaches the surface, there would have been venting of the foam associated with effusive emplacement of the mare [11].

The newly identified vent features are located along "shallow v" fractures. These fractures have a "v" shaped cross-sectional profile and are less than 50 m in depth; they are interpreted to form via brittle fracturing of the crater floor during the uplift associated with sill formation. The vents are irregularly spaced along the "shallow v" fractures, have depths of greater than 100 m for the entire length of the vent, and have neither a low-albedo deposit, nor a spectroscopically identifiable deposit of pyroclastic material. We interpret these features to form from the venting of a pure gas or a highly gas-rich foam, likely during the initial outward expansion of the magmatic foam during the sill formation process. We also hypothesize that this processes was precipitated by the downward propagation of the fracture tapping the gas-rich foam [11], and would have erupted primarily gas and wall-rock material, similar to deposits in vulcanian-style eruptions.

Variations in Eruption Styles: These newly identified vents in Humboldt are most morphologically similar to the relatively newly identified vents in Alphonsus (Fig. 1b) [9], being smaller than previously identified vents, located along fractures, and broadly lacking sur-

rounding deposits of lower albedo material. This suggests venting of a gas-rich phase and collapse of wall material [15, 16]. These 2 vents without dark halo deposits differ from the classically recognized dark halo deposit vents within Alphonsus crater both in size and in amount of pyroclastic material ejected in the eruption. The low albedo annuli of the other deposits suggest a larger amount of entrained solidified basaltic fragments, an observation corroborated by the identification of olivine in these deposits [10, 17]. The radial extent of pyroclastic material can be used to infer eruption velocity and gas and pyroclast volume fractions for the eruption [e.g. 15, 18, 19]. This has been done for several of the deposits within Alphonsus [11, 20], suggesting gas volume fractions of ~0.03-0.04. The similarity in gas volume fraction between deposits is unsurprising given the relative similarity in deposit radius [5]. These data suggest that these deposits were formed from the eruption of a relatively homogenous magmatic foam layer. We are currently investigating the morphologies of the fractures in Alphonsus and assessing stratigraphic relationships between the fracture segments hosting the deposits without low albedo annuli and the fracture segments with low albedo annuli which could be suggestive of a temporal evolution in the eruption processes.

Conclusions: Lunar pyroclastic deposits have been classically divided into two size categories [5]: large regional deposits formed by fire-fountaining [7], and smaller localized deposits formed by vulcanian eruptions [8]. We performed a detailed morphologic analysis of fracture and vent styles in the floor-fractured craters Humboldt and Alphonsus to assess variations in eruption style and how the eruptions relate to the overall formation and evolution of the magmatic intrusion. We find evidence that the majority of volcanic vent morphologies formed syn-emplacement with the sill and that, variations in gas content could be indicative of different phases of foam evolution and intrusion degassing and venting.

References: [1] Schultz, P. H. (1976) *The Moon 15*, 241-273. [2] Jozwiak, L. M., et al. (2012) *JGR, 117*, E11. [3] Jozwiak, L. M., et al. (2015) *Icarus, 248,* 424-447. [4] Gaddis, L. R., et al. (1985) *Icarus 61*, 461-489. [5] Gaddis, L. R., et al. (2003) *Icarus 161*, 262-280. [6] Head, J. W. (1975) *Rev. Geophys. And Space Phys. 14*, 265-300. [7] Wilson, L., Head, J. W. (1981) *JGR 86*, 2971-3001. [8] Head, J. W. and Wilson, L. (1979) *Proc. Lunar Planet. Sci. Conf. 10th*, 2861-2897. [9] Gaddis, L. R., et al. (2011) *LPSC XLII*, Abstract #2691. [10] Hawke, B. R., et al. (1989) *Proc. Lunar Planet Sci. Conf. 19th*, 255-268. [11] Jozwiak, L. M., et al. (2016) *Manuscript in prep*. [12] Haruyama, J., et al. (2009) *LPSC XL*, Abstract #1553. [13] Barker, M. K., et al. (2014) *LPSC XLV*, Abstract #1777. [14] Pollard, D. D., Johnson, A. M. (1973) *Tectonophysics 18*, 311-354. [15] Wilson, L., Head, J. W. (2015) *Icarus, In Press.* [16] Head, J. W., Wilson, L. (2016) *LPSC XLVII*, Abstract #1189. [17] Coombs, C. R., et al. (1990) *Proc. Lunar Planet Sci. Conf. 20th*, 339-353. [18] Wilson, L. and Head, J.W. (2003) *GRL 30*, 1605. [19] Wilson, L., et al. (2014) *LPSC XLV*, Abstract #1223. [20] Jozwiak, L. M., et al. (2015) *LPSC XLVI*, Abstract #1580.

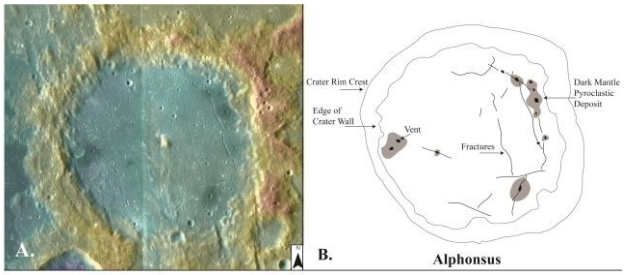

Figure 1: Lunar floor-fractured crater Alphonsus (D = 119 km) (13.4° S, 2.8° W). A) Image of Alphonsus crater overlain on topography (red high, blue low). The floor fractures and several of the low albedo pyroclastic deposits are visible around vents. B) Geologic sketch map of the volcanic morphologies within Alphonsus including: vents, fractures, and dark mantle pyroclastic deposits. The two newly identified vents within Alphonsus [8] can be seen lacking a surrounding dark mantle deposit. Figure from Jozwiak et al. (2015) [3].

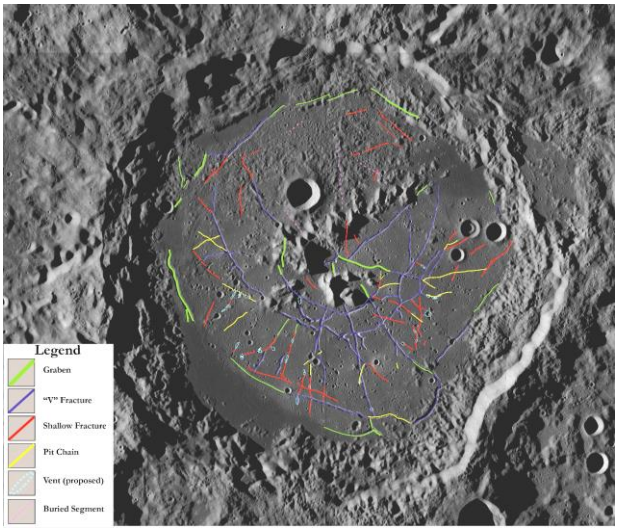

Figure 2: Image of Humboldt crater (D = 208 km) (27.2° S, 80.9° E) with mapped fracture morphologies. The graben-style fractures (green) are located along the edge of the crater floor, and are superposed and embayed by the wall-adjacent mare deposits. The center of the crater floor is dominated by deep v-shaped cross-sectional fractures (blue), interpreted to result from upward bending of the crater floor. The v-shaped fractures grade outward into shallow v fractures (red) which suggest lower degrees of bending away from the center of the crater. The newly identified vent features (teal) are predominately located along the shallow fracture segments, and are interpreted to result from degassing of gas-rich magmatic foam which is tapped by the downward propagating fracture. The map is composed of Kaguya Terrain Camera night images [11].